

## Modeling observed chaotic oscillations in bursting neurons: the role of calcium dynamics and $IP_3$

Martin Falcke<sup>1</sup>, Ramón Huerta<sup>2,3</sup>, Mikhail I. Rabinovich<sup>2</sup>,  
 Henry D. I. Abarbanel<sup>4,5</sup>, Robert C. Elson<sup>6</sup>, Allen I. Selverston<sup>6</sup>

<sup>1</sup> Max Planck-Institute for the Physics of Complex Systems, Nöthnitzer Strasse 38, 01187 Dresden, Germany

<sup>2</sup> Institute for Nonlinear Science, University of California at San Diego, La Jolla, CA 92093-0402, USA

<sup>3</sup> E.T.S Ingeniería Informática, Universidad Autónoma de Madrid, 28049 Madrid, Spain

<sup>4</sup> Department of Physics, University of California at San Diego, La Jolla, CA 92093-0402, USA

<sup>5</sup> Marine Physical Laboratory, Scripps Institution of Oceanography, University of California, San Diego, La Jolla, CA 92093-0402, USA

<sup>6</sup> Department of Biology, University of California, San Diego, La Jolla, CA 92093-0402, USA

Received: 24 February 1999 / Accepted in revised form: 17 December 1999

**Abstract.** Chaotic bursting has been recorded in synaptically isolated neurons of the pyloric central pattern generating (CPG) circuit in the lobster stomatogastric ganglion. Conductance-based models of pyloric neurons typically fail to reproduce the observed irregular behavior in either voltage time series or state-space trajectories. Recent suggestions of Chay [Biol Cybern 75: 419–431] indicate that chaotic bursting patterns can be generated by model neurons that couple membrane currents to the nonlinear dynamics of intracellular calcium storage and release. Accordingly, we have built a two-compartment model of a pyloric CPG neuron incorporating previously described membrane conductances together with intracellular  $Ca^{2+}$  dynamics involving the endoplasmic reticulum and the inositol 1,4,5-trisphosphate receptor  $IP_3R$ . As judged by qualitative inspection and quantitative, nonlinear analysis, the irregular voltage oscillations of the model neuron resemble those seen in the biological neurons. Chaotic bursting arises from the interaction of fast membrane voltage dynamics with slower intracellular  $Ca^{2+}$  dynamics and, hence, depends on the concentration of  $IP_3$ . Despite the presence of 12 independent dynamical variables, the model neuron bursts chaotically in a subspace characterized by 3–4 active degrees of freedom. The critical aspect of this model is that chaotic oscillations arise when membrane voltage processes are coupled to another slow dynamic. Here we suggest this slow dynamic to be intracellular  $Ca^{2+}$  handling.

### 1 Introduction

Even when deprived of noisy inputs, many neurons spike in variable or irregular patterns. Such activity is

difficult to simulate in model neurons built according to the Hodgkin-Huxley formalism of membrane conductances. It is the goal of this article to show that a conductance-based neuron model can generate complex variable burst patterns when augmented by biologically plausible intracellular  $Ca^{2+}$  dynamics. Our modeling work is motivated by the experimental observation of irregular bursting in synaptically isolated neurons of the pyloric central pattern generator (CPG) circuit of the crustacean stomatogastric ganglion (STG) (Bal et al. 1988). Analyses of voltage time series of one such neuron (the lateral pyloric, LP) have shown a wide region of voltage-dependent behavior in which the cell generates bursts of highly variable duration in a seemingly chaotic pattern (Abarbanel et al. 1996). The chaotic spiking-bursting behavior of living STG neurons is not adequately reproduced by existing conductance-based models (Buchholtz et al. 1992; Turrigiano et al. 1995). Simplified models such as those of Hindmarsh and Rose (1984) or Chay (1996) are useful for phenomenological analysis (Abarbanel et al. 1996), but to gain a deeper understanding one must build realistic models that incorporate membrane conductances and include spatial aspects of the neuron and slower intracellular processes. In this article the source of additional slow dynamics is  $Ca^{2+}$  exchange between the cytosol and intracellular stores.

We suggest a two-compartment model of the STG neuron. The two compartments reflect the spatial structure of the neuron. An “axon” compartment is responsible for spiking activity while a “soma/neuropil” compartment produces slower voltage oscillations (underlying bursting activity) (Hartline and Graubard 1992). The simulation of membrane conductances is based on previous descriptions (see Buchholtz et al. 1992; Turrigiano et al. 1995). The soma/neuropil compartment also incorporates  $Ca^{2+}$  exchange between the endoplasmic reticulum (ER) and the cytosol, regulated by an intracellular messenger inositol 1,4,5-trisphosphate ( $IP_3$ ). These complex calcium dynamics

---

Correspondence to: M. Falcke  
 (e-mail: falcke@mpipks-dresden.mpg.de)

change the behavior of the membrane voltage, producing irregular bursting activity with clear qualitative and quantitative similarities to experimental observations.

The calcium release channel of the ER is assumed to be an inositol 1,4,5-trisphosphate receptor channel (IP<sub>3</sub>R), as modeled by Li et al. (1997). The presence of this channel remains hypothetical for STG neurons but has been demonstrated in several other neuronal types (Otsu 1990; Satoh 1990; Walton 1991). IP<sub>3</sub> is produced in a bifurcating pathway together with diacylglycerol when agonists bind to a family of G-protein-linked receptors or to receptors linked by tyrosine kinase (Berridge 1987, 1993a,b). IP<sub>3</sub> functions to release Ca<sup>2+</sup> from the ER (Berridge 1987) and plays a role in fertilization and development, cell growth, cell transformation, neuromodulation, and plasticity (Bootman and Berridge 1995). In particular, it has been suggested that IP<sub>3</sub> modulates Ca<sup>2+</sup> oscillations in several cells (Berridge 1987). Receptors for IP<sub>3</sub> differ with respect to their sensitivity and conductance. However, the essential dynamics of interaction between membrane voltage and intracellular Ca<sup>2+</sup> most likely do not depend on these specific details, as long as the Ca<sup>2+</sup>-releasing channel receives feedback (1) from cytosolic Ca<sup>2+</sup> (calcium-induced calcium release) and (2) from the filling state of the intracellular Ca<sup>2+</sup> store. These conditions are met by different IP<sub>3</sub> receptors (Pozzan 1994). We have adopted a model of IP<sub>3</sub>R function recently proposed by Li et al. (1997).

Here we report that varying the concentration of IP<sub>3</sub>, [IP<sub>3</sub>] allows the model neuron to produce both regular oscillations and chaotic behavior. These findings suggest new experiments to elucidate Ca<sup>2+</sup> oscillations and the impact of IP<sub>3</sub> in the biological neurons. Furthermore we provide a nonlinear dynamical comparison (Abarbanel 1996) of the output of the model and of the pyloric CPG neuron as measured in our laboratory. This quantitative comparison reveals that each produces low-dimensional dynamics with 3 or 4 active degrees of freedom. The model has 12 independent dynamical variables, and these contract to a subspace of the full state space of the system.

We have identified a biologically plausible source – slow internal Ca<sup>2+</sup> exchange – for the production of chaotic behavior in otherwise regular Hodgkin-Huxley dynamics. At present we do not have direct experimental evidence to support our proposal, although exploratory experiments are underway. However, the key ingredient of this article is the understanding that additional slow dynamics are essential if conductance-based models are to simulate (qualitatively and quantitatively) the complex irregular spiking and bursting activity observed in the STG neurons.

## 2 The model

The equations of the mathematical model are given in Appendix B. There are two compartments in our model. With one we represent the neuropil and the soma

[membrane voltage  $V(t)$ ], and with the other we represent the axon [membrane voltage  $V_1(t)$ ]. We locate the slow wave generator for voltage dynamics in the soma/neuropil compartment and the fast generator for spikes in the axonal compartment. The action potentials generated in the axon spread passively back through the neuropil, reaching the soma (the site of intracellular recordings in experiments) with a final amplitude of about 10 mV. There, they appear as spikes on top of the slow oscillations generated in the soma/neuropil compartment (see Fig. 1). This distribution of conductances and these electrotonic properties resemble those of the biological neurons in the stomatogastric ganglion (Hartline and Graubard 1992).

Our currents are based on previous descriptions (Buchholtz et al. 1992; Turrigiano et al. 1995) but are restricted to those that we assume are indispensable for generating appropriate voltage activity. A coupling current,  $I_{V,V_1}$ , flows between the two compartments in proportion to their voltage difference. These voltages are also determined by a specific set of membrane currents in each compartment.

There are five membrane currents in the soma/neuropil compartment:

- Small maximum conductance Ca<sup>2+</sup> current  $I_{Ca1}$ : This current has a fast low voltage activation. It inactivates on a slower time scale. The major function of  $I_{Ca1}$  is to initiate the transition from low membrane voltage to the plateau level.
- Large maximum conductance Ca<sup>2+</sup> current  $I_{Ca2}$ : This current creates the plateau. It activates at higher voltage than  $I_{Ca1}$  and does not inactivate.
- Hyperpolarization-activated inward current  $I_h$ : This current is responsible for restorative depolarization following a strong hyperpolarization of the membrane.
- Ca<sup>2+</sup> dependent K<sup>+</sup> current  $I_{K(Ca)}$ : This current activates at high voltage. It increases with cytosolic [Ca<sup>2+</sup>]. It is crucial for the termination of the plateau.
- Leak current  $I_l$ .

Three membrane currents underlie spike generation in the axon compartment:

- Fast Na<sup>+</sup> current  $I_{Na}$ : This current generates spikes, if  $V_1(t)$  is above firing threshold.
- Delayed rectifier K<sup>+</sup> current  $I_{Kd}$ : This current repolarizes the membrane during spike generation.
- Leak current  $I_l$ .

The soma/neuropil compartment also incorporates intracellular Ca<sup>2+</sup> dynamics based on the model of Li et al. (1997). Cytosolic [Ca<sup>2+</sup>] is determined by influx across the plasma membrane ( $I_{Ca2}$  and  $I_{Ca1}$ ), by uptake and release from the ER, and by extrusion by a plasma membrane pump and a plasma membrane Na<sup>+</sup>-Ca<sup>2+</sup> exchanger. The model for Ca<sup>2+</sup> release from the ER is based on the IP<sub>3</sub>-sensitive channel. There are three binding sites assumed on the IP<sub>3</sub> receptor (IP<sub>3</sub>R): an activating site for IP<sub>3</sub>, an activating site for Ca<sup>2+</sup>, and an inhibiting site for Ca<sup>2+</sup>. If IP<sub>3</sub> and Ca<sup>2+</sup> are bound to the activating site, the channel is

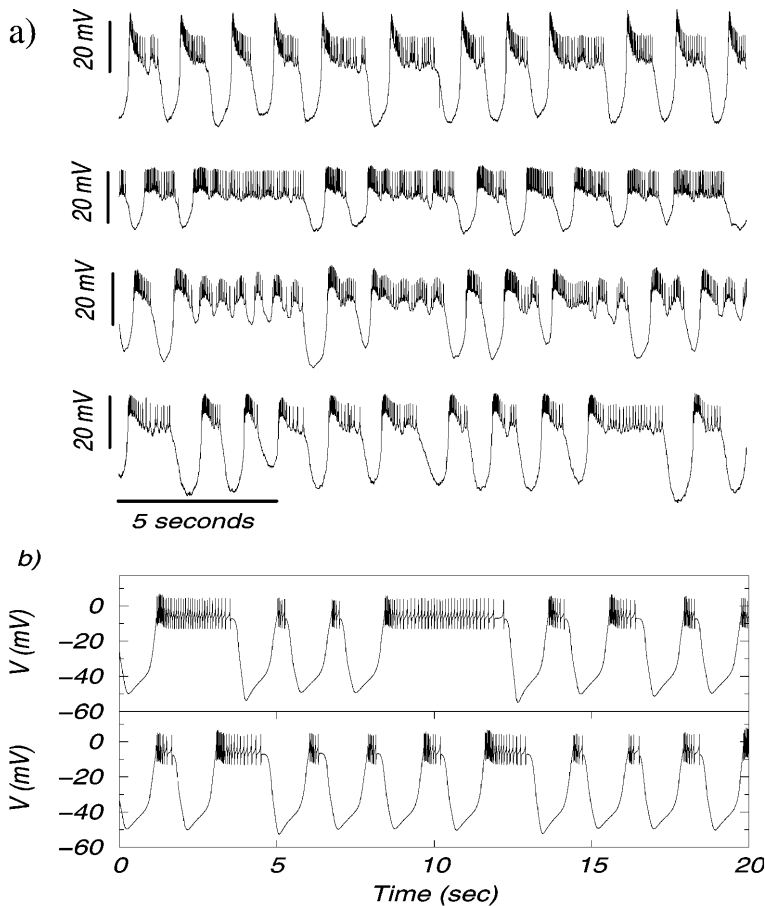


**Fig. 1.** **a** Experimental time series of the soma membrane voltage of the lateral pyloric (LP) neuron in four different preparations. *Experimental methods:* The stomatogastric nervous system was removed from adult spiny lobsters, *Panulirus interruptus*, and prepared for electrophysiological recordings (Mulloney and Selverston 1974). Using standard pharmacological and cell-killing techniques (Miller and Selverston 1979; Bal et al. 1988), the LP neuron was isolated from synaptic inputs provided by other neurons of the pyloric circuit. Descending modulatory input from anterior ganglia was retained. Under these conditions, LP typically generated an irregular pattern of slow voltage oscillations and bursts of spikes. **b** Calculated time series of the soma membrane voltage  $V$  in the model neuron with  $IP_3 = 0.29 \mu\text{M}$  (top panel),  $IP_3 = 0.35 \mu\text{M}$  (bottom panel)

open and releases  $\text{Ca}^{2+}$  out of the ER. The binding of  $\text{Ca}^{2+}$  to the inhibiting site is considerably slower and closes the channel. In this way the channel opens at low concentration of cytosolic  $\text{Ca}^{2+}$  and closes at high  $[\text{Ca}^{2+}]$ . The refractory state of the receptor is determined by the dissociation of  $\text{Ca}^{2+}$  from the inhibiting site.  $\text{Ca}^{2+}$ -ATPases pump  $\text{Ca}^{2+}$  back into the ER. Since in the framework of this model  $[IP_3]$  is assumed to be constant (Li et al. 1997), changes of the state of the receptor are controlled by  $[\text{Ca}^{2+}]$  only.

### 3 Behavior of the model

In Fig. 1a we show sample recordings of soma voltage taken from the LP neuron of the stomatogastric ganglion following the removal of strong synaptic inputs from other pyloric circuit neurons. These are compared with segments of a soma voltage time series generated by the model neuron (Fig. 1b). The main characteristic common to both sets is variability of burst duration. The variability seen in experimental recordings is compared to the model results in Fig. 2. Most burst periods of the experimental time series are in the range of 1–3 s and for the model in the range of 1.5–3 s with the most frequent period of about 1.7 s. The maximum periods reach about 6 s in the experimental time series and about 5 s in the model simulations.

In the model neuron, the soma compartment produces plateau depolarizations that drive the axon compartment to generate bursts of spikes. The plateau potential is maintained by the competition between the inward currents  $I_{\text{Ca}1}$  and  $I_{\text{Ca}2}$  on one side and the outward currents  $I_{\text{K}(\text{Ca})}$  and  $I_l$  and the coupling to the axon compartment on the other side. Among the two  $\text{Ca}^{2+}$

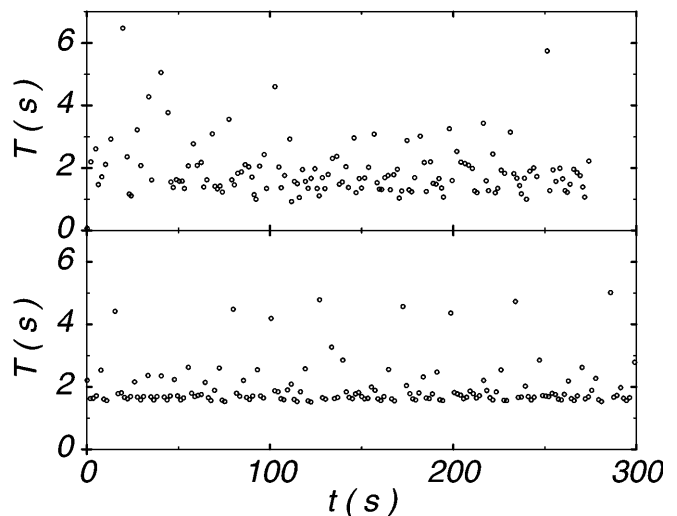


**Fig. 2.** *Top* Experimentally measured burst periods. *Bottom* Calculated burst periods with  $IP_3 = 0.354 \mu\text{M}$

currents,  $I_{Ca1}$  initiates, while  $I_{Ca2}$  helps to sustain the plateau. The magnitude of  $I_{K(Ca)}$  depends on both voltage and cytosolic  $[Ca^{2+}]$ . The influx of  $Ca^{2+}$  during the plateau increases this current, leading finally to plateau termination. The voltage then drops to values of about  $-45$  mV. Cytosolic  $[Ca^{2+}]$  decreases because the  $[Ca^{2+}]$  currents deactivate and because  $Ca^{2+}$  is pumped out of the cell and into the ER. Thereafter,  $I_{K(Ca)}$  decreases and the voltage rises slowly until activation of  $I_{Ca1}$  initiates the next voltage plateau. In the course of a bursting cycle, cytosolic  $[Ca^{2+}]$  varies with an amplitude of 20–40 nM.

During steady state bursting,  $[Ca^{2+}]$  in the ER (luminal  $[Ca^{2+}]$ ) oscillates with a small amplitude around an average filling state (Fig. 3, bottom). The average filling state has a strong impact on the oscillations of cytosolic  $[Ca^{2+}]$ . This can be seen by starting the simulation at low luminal  $[Ca^{2+}]$  and allowing the ER to fill up. As luminal  $[Ca^{2+}]$  increases, the amplitude and period of cytosolic  $[Ca^{2+}]$  oscillations decrease (see Fig. 3, top). This allows for a feedback of the filling state of the ER to the membrane oscillations and the  $Ca^{2+}$  flux across the plasma membrane. At very low

luminal  $[Ca^{2+}]$ , the model undergoes relaxation oscillations. Within one period, cytosolic  $[Ca^{2+}]$  has a short peak but is low during the longer part of the oscillation. Hence,  $I_{K(Ca)}$  cannot terminate the voltage plateau for most of the period.  $I_{Ca2}$  stays high providing large  $Ca^{2+}$  flux into the cell. Additionally,  $[Ca^{2+}]$  extrusion by the cell membrane pump and exchanger is low. The  $[Ca^{2+}]$  entering the cell is taken up by the ER raising the filling state. This leads to oscillations with a more sinusoidal shape and relatively shorter phases of low cytosolic  $Ca^{2+}$  (Fig. 3, bottom). In turn this decreases the amount of  $Ca^{2+}$  entering the cell within one oscillation period. The asymptotic state has no average net flux of  $Ca^{2+}$  across the cell membrane within one oscillation. [This mechanism of communication between the ER and the cell membrane was described by Li et al. (1997) for gonadotrophs.] Thus, the ER controls the character of the oscillations so that it stabilizes its filling state.

The  $IP_3$  concentration determines the value of the filling state being stabilized and therefore the intrinsic time scale of the oscillations of the  $Ca^{2+}$  system. Depending on the value of  $[IP_3]$ , the model neuron can

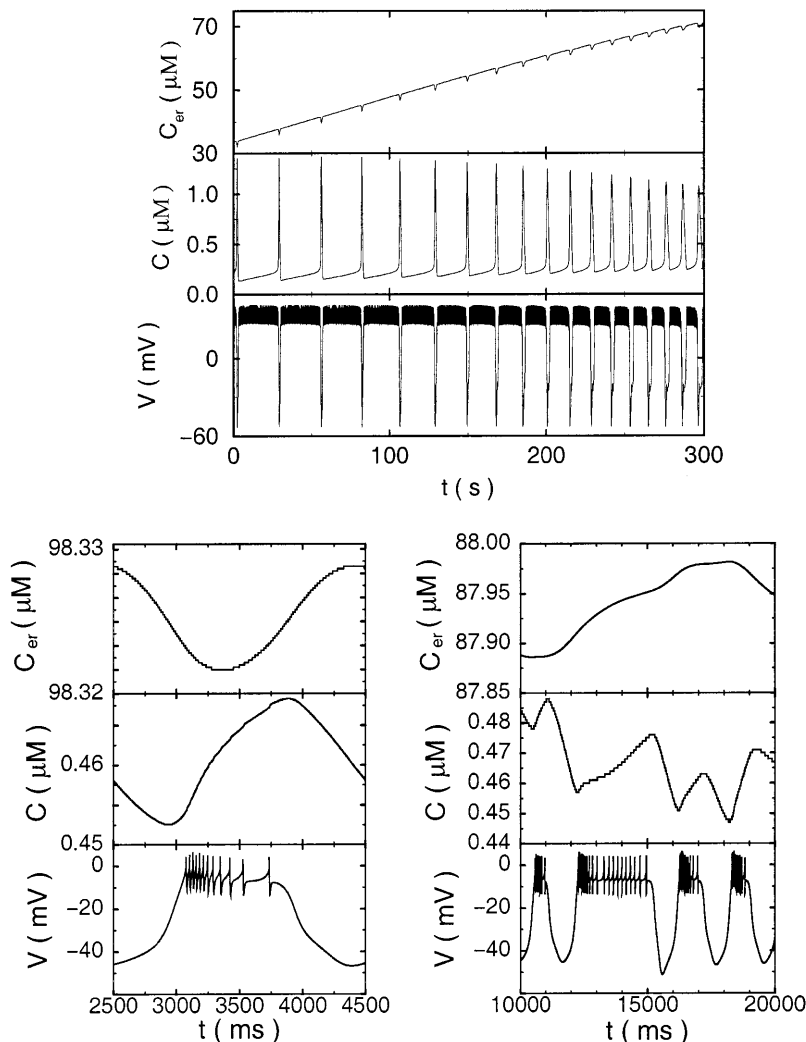


**Fig. 3.** *Top* Transient behavior of the model starting from low luminal  $Ca^{2+}$   $C_{er}$  ( $C$  cytosolic  $Ca^{2+}$ ,  $V$  soma membrane voltage;  $IP_3 = 0.272 \mu M$ ). The asymptotic state reached after the transient behavior is shown in the bottom left figure. *Bottom* Phase relation between luminal  $Ca^{2+}$  ( $C_{er}$ ), cytosolic  $Ca^{2+}$  ( $C$ ) and the membrane voltage of the soma  $V$  for regular oscillations (*left*  $IP_3 = 0.272 \mu M$ ) and chaotic behavior (*right*  $IP_3 = 0.354 \mu M$ ). The phase relation between  $V$  and  $C$  is always preserved:  $C$  has a minimum at the beginning of the voltage plateau and a maximum at the end.  $C_{er}$  oscillates with the same period as  $C$  and  $V$ . The phase relation between  $V$  and  $C$  on one side and  $C_{er}$  on the other side is lost in the chaotic regime (*bottom right*).  $C_{er}$  changes on a time scale of a few bursts. Note that  $C_{er}$  increases monotonously during the second and third bursts (*bottom right*) before it starts to decrease again

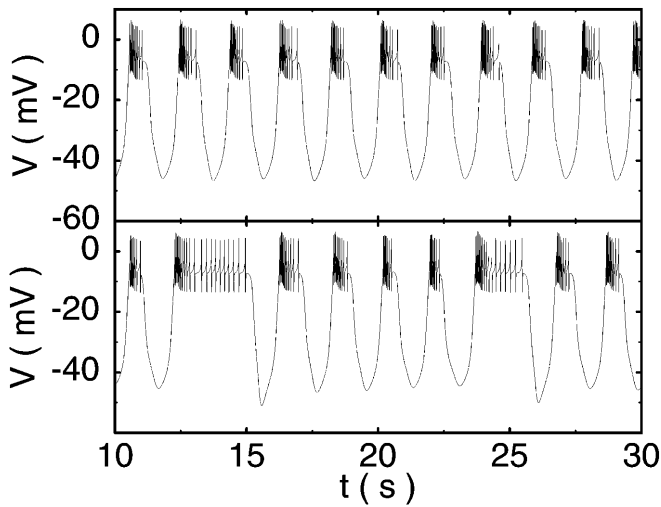


**Fig. 4.** Calculated time series of the soma membrane voltage  $V$  with  $IP_3 = 0.272 \mu M$  (top) and  $IP_3 = 0.354 \mu M$  (bottom)

generate regular oscillations as well as chaotic behavior. At low  $[IP_3]$ , regular oscillations occur (Fig. 4, top;  $[IP_3] = 0.272 \mu M$ ). Increasing  $[IP_3]$  causes a transition to chaotic behavior (Fig. 4, bottom;  $[IP_3] = 0.354 \mu M$ ). This transition occurs when the intrinsic time scale of the  $Ca^{2+}$  subsystem approaches the intrinsic time scale of the voltage oscillations. It is the interaction of the intracellular  $Ca^{2+}$  dynamics with membrane voltage dy-

namics that creates chaotic bursting. When uncoupled from each other, neither subsystem behaves chaotically. This is evocative of the general case of coupling between a slow oscillator and a system moving on a limit cycle close to a homoclinic orbit, which might lead to chaos (Gaponov-Grekhov 1992; Arnold 1993).

The oscillations of cytosolic  $[Ca^{2+}]$  couple the luminal  $[Ca^{2+}]$  to the membrane dynamics and vice versa. During regular bursting, luminal  $[Ca^{2+}]$  and cytosolic  $[Ca^{2+}]$  oscillate with the same period. Cytosolic  $[Ca^{2+}]$  reaches its maximum at the end of the burst, luminal  $[Ca^{2+}]$  following with a certain phase lag (Fig. 3, bottom left). During chaotic bursting, however, this phase relation is lost and luminal  $[Ca^{2+}]$  oscillates irregularly on the time scale of several burst periods (Fig. 3, bottom right). The amplitude of these slow oscillations is larger than those that occur during regular bursting. These slow oscillations of luminal  $[Ca^{2+}]$  are essential for chaotic bursting. If one sets luminal  $[Ca^{2+}]$  to a constant value, a transition to regular oscillations occurs. Hence, regular oscillations can occur without luminal  $[Ca^{2+}]$  oscillations but chaos cannot.

Figure 5 shows the range of  $IP_3$  concentrations and injected currents at which chaotic bursting was found. Chaotic attractors were identified by inspection of a parametric Poincaré section that shows a dense distribution of points for chaotic behavior. This was corroborated for sample time series by calculations of the Lyapunov exponents (see Sect. 4 below). In Fig. 5a we

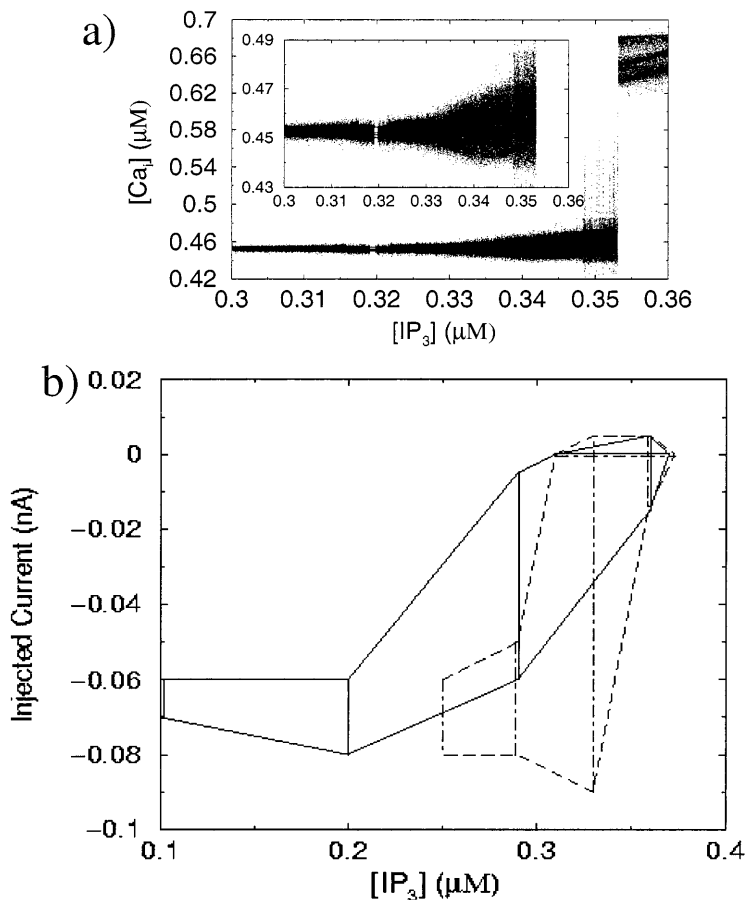


**Fig. 5.** **a** One-parameter Poincaré section for increasing values of  $[IP_3]$ . The chaotic regime widens as  $[IP_3]$  is increased. The inserted figure is a blowup of the region of normal operation. **b** Values of  $[IP_3]$  and injected current for which chaotic behavior was found. The vertical lines show the parameter scans we performed. Full lines: Calculations with the parameters given in Appendix B. Dash-dotted lines: Results with  $Ca^{2+}$  removal parameters:  $K_{pmp} = 0.5 \mu M$ ,  $K_{pmex} = 1.2 \mu M$ ,  $v_{pmp} = 0.0202 \mu M s^{-1}$ ,  $v_{pmex} = 0.606 \mu M s^{-1}$ . Additionally the time scale of the activation of  $I_{Ca2}$  ( $m_{Ca2}$ ) was increased by a factor 1.13

show a one-parameter Poincaré section, plotting cytosolic  $[Ca^{2+}]$  values as a function of  $[IP_3]$  ( $I_{dc} = 0$ ). Chaotic oscillations were observed for  $[IP_3]$  between  $0.310 \mu M$  and  $0.373 \mu M$ . This range extended down to  $[IP_3] \approx 0.10 \mu M$  upon injection of negative dc (Fig. 5b, solid outlines). Conversely, the range was compressed when we increased the slope dependence of  $Ca^{2+}$  extrusion upon cytosolic  $[Ca^{2+}]$  (Fig. 5b, dashed lines). The results obtained with the model neuron differ from the experimental observations in the parameter region where the values of cytosolic  $[Ca^{2+}]$  amplitudes are high ( $0.7 \mu M$ , large  $[IP_3]$ ). There, the period of the simulated oscillations increases to about 10 s and the voltage overshoots to  $+20$  mV at the beginning of the bursts. This behavior was not observed in experiments.

A further test of the model was provided by introducing dc current into the soma/neuropil compartment, as in experiments reported in Abarbanel et al. (1996). We observe the following general scenario (Fig. 6). The membrane voltage stays at about  $-45$  mV for very negative injected currents ( $\leq -0.09$  nA). At large positive injected currents the model spikes tonically. At intermediate values, chaotic behavior or regular oscillations are observed. The period of the regular oscillations decreases with increasing injected current, accompanied by an increase of the minima of the membrane voltage  $V(t)$  from  $-45$  mV to  $-30$  mV. These trends resemble experimental observations. The major difference to experimental measurements is the existence of a regime of regular bursting between the chaotic regime and the quiescent state in experimental neurons that was not found in the model. There, the chaotic behavior extends down to the quiescent state. As the model neuron was depolarized by positive dc current, we could observe period-doubling bifurcations (e.g. Fig. 6,  $0.04$  nA).

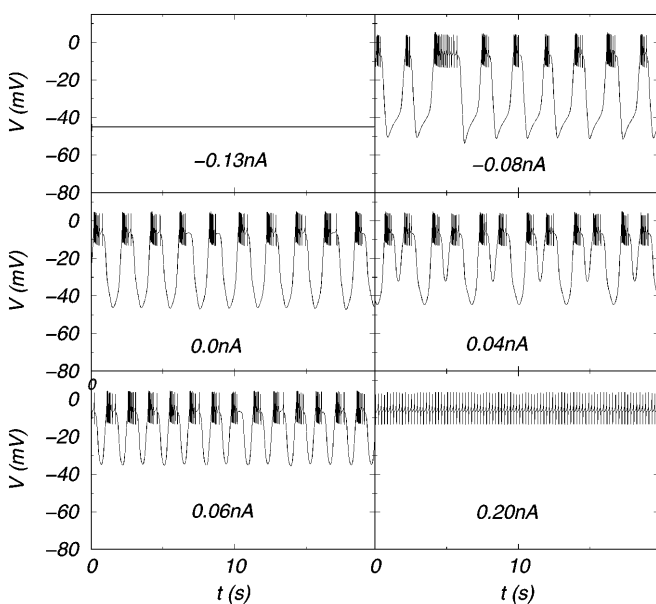


**Fig. 6.** Calculated membrane voltage time series with injected currents at  $IP_3 = 0.29 \mu M$ . The values of the injected currents are given in the figures

#### 4 Comparison of voltage time series in model and experimental data

For quantitative comparison of model and experimental time series, we used a standard set of nonlinear analysis algorithms (Abarbanel 1996). The state space of the system (model cell or biological neuron) can be reconstructed from measurements of an observed variable using the method of time delays. This reconstruction proceeds by forming  $d$ -dimensional vectors from membrane voltage data  $V(t) = V(n) = V(t_0 + n\tau_s)$  starting at some time  $t_0$  and sampling it every  $\tau_s$ . In both our experimental observations and in our model calculations  $\tau_s = 0.5$  ms. These vectors take the form:

$$\mathbf{y}(n) = [V(n), V(n+T), V(n+2T), \dots, V(n+(d-1)T)] ,$$

where the integer  $T$  is the number of time steps of length  $\tau_s$  between components of the state vector  $\mathbf{y}(n)$ .

We determine  $T$  by asking when the components of  $\mathbf{y}(n)$  are independent of one another in a nonlinear fashion. For this purpose we plot the average mutual information between measurements as a function of  $T$  and choose the  $T$  value for which the information reaches its first minimum. The theory of state space reconstruction indicates that all properties of the underlying system deduced from time delay plots should be independent of  $T$  (Takens 1981). Numerically one does not find this for very small or very large  $T$ , but experience (Abarbanel 1996) shows the choice of the first minimum of average mutual information to work quite well. However, since this is not a rigorous result but provides an orientation for the choice of  $T$  only, the estimations are performed not only for this choice of  $T$  but also the surrounding values are used to assure the results. Figure 7 (top) shows the average mutual information evaluated from a long time series from a synaptically isolated LP neuron. A first minimum is visible at  $T = 11$  or  $5.5$  ms. In Fig. 7 (bottom) we show the same quantity for the model neuron in its chaotic regime ( $[IP_3] = 0.354 \mu M$ ). A first minimum occurs at  $T = 5$ .

The dimension of the reconstructed state space  $d_E$  is estimated by the method of false nearest neighbors (Abarbanel 1996). Figure 8 (top) shows that, for the biological data, the number of false nearest neighbors declines to zero at  $d_E = 7$ . In Fig. 8 (bottom), we show the same quantity for the model output. Here it is possible to conclude that the percentage of false nearest neighbours is zero at  $d_E = 6$ , but for ‘‘safety’’ we have used  $d_E = 7$  in subsequent calculations.

Once this global dimension has been determined, we would like to know what dimension is required locally by the dynamics. Dissipative dynamical systems possess an attractor whose dimension is smaller than that of the whole state space (and typically noninteger). To estimate this load dimension,  $d_L$ , we use the method of local false nearest neighbors, in which we test our ability to predict the local evolution of the attractor, as a function of dimension and the number of neighboring points (Abarbanel 1996). Figure 9 (top) shows the results of this

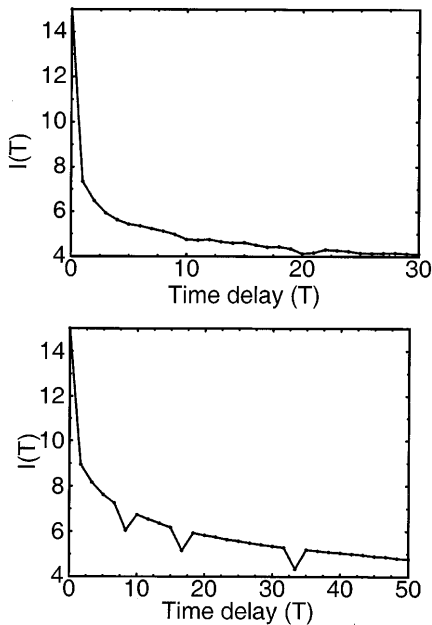


**Fig. 7.** Average mutual information for the LP neuron. *Top* Evaluated from experimental data. *Bottom* Evaluated from the model with  $IP_3 = 0.354 \mu\text{M}$

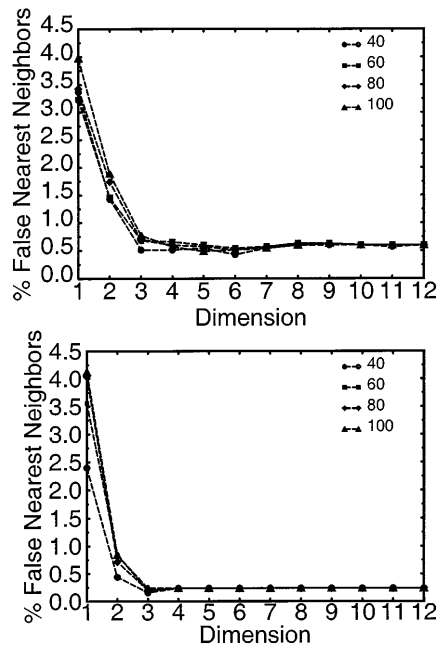


**Fig. 9.** Local false nearest neighbors for the LP neuron including 40, 60, 80, and 100 neighbors in the calculation. *Top* Evaluated from experimental data. *Bottom* Evaluated from the model with  $IP_3 = 0.354 \mu\text{M}$

calculation using the experimental data; Figure 9 (bottom) comes from analysis of the model data. In each case the quality of the prediction becomes independent of dimension and number of neighbors at  $d_L = 3$ .

Thus, both the observed and the model data can be described by three dynamical variables. This is a re-

markable property of either data set, and more so as they agree. In the biological neuron there are many ion channels and intracellular dynamical processes operating. Similarly, the model neuron involves many membrane currents as well as critical  $Ca^{2+}$  dynamics (see Appendix B). Yet, in both, only three dynamical variables determine the time course of membrane potential. The analysis does not tell us which those three are, but it does serve as a guide for our search.

Finally, we evaluate the spectrum of  $d_L = 3$  Lyapunov exponents. These quantities determine the stability of neural oscillations. Since we are dealing with dissipative systems that can be described by sets of differential equations, we expect one exponent to be zero and their sum to be negative. The presence of a positive exponent indicates that a system is chaotic. Details on calculating the Lyapunov exponent spectrum are described elsewhere (Abarbanel 1996). Figure 10 (top) shows the exponents for the experimental data. We see one positive exponent ( $\lambda_1 = 0.4$ ), one exponent near zero ( $\lambda_2 = 0.07$ ), and one negative exponent ( $\lambda_3 = -0.57$ ); the sum of the exponents is negative. The so-called Lyapunov dimension,  $D_L$ , is an estimate of the fractional dimension of the system attractor: here  $D_L = 2.8$ . For the model data (Fig. 10, bottom), we found  $\lambda_1 = 0.12$ ,  $\lambda_2 = -0.0062$ , and  $\lambda_3 = -0.20$  for a  $D_L = 2.6$ . This is an excellent agreement between the experimental data and the model. It is possible that another value for  $[IP_3]$  might yield still closer agreement between Lyapunov exponents. Although we have not explored the full range of dynamical behaviors, our results indicate that the model captures the overall dynamical aspects of the observed data.

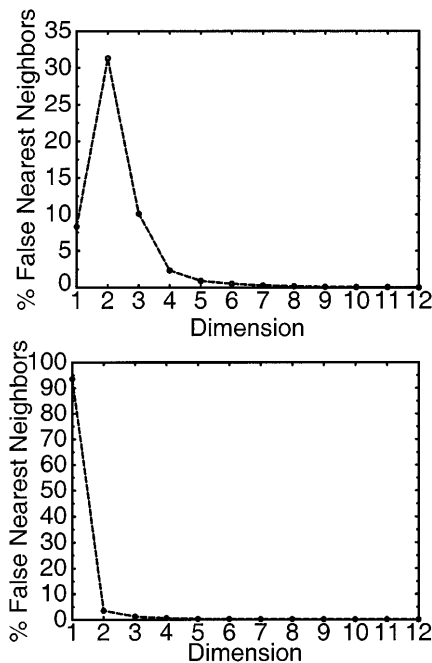


**Fig. 8.** Global false nearest neighbors for the LP neuron. *Top* Evaluated from experimental data. *Bottom* Evaluated from the model with  $IP_3 = 0.354 \mu\text{M}$

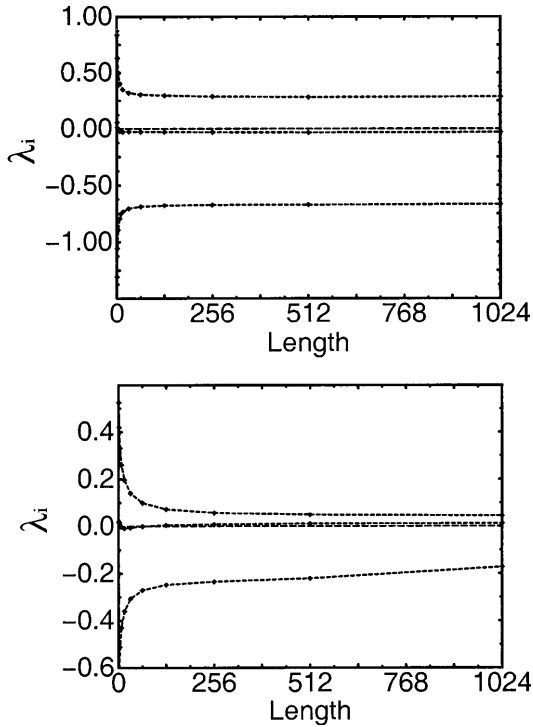


**Fig. 10.** The spectrum of Lyapunov exponents for the LP neuron. Each was evaluated in  $d_E = 7$  and  $d_L = 3$  as suggested by the previous results. *Top* Evaluated from experimental data. *Bottom* Evaluated from the model with  $IP_3 = 0.354 \mu\text{M}$

Finally, since the dimension is low, we can exhibit the shape of the reconstructed attractors. Figure 11 shows the similar topology of attractors reconstructed in three-dimensional state space (using membrane voltage  $V(t)$  and its time delays  $\mathbf{y}(t) = [V(t), V(t - T), V(t - 2T)]$ ) for the case of the experimental recording and the model data.

## 5 Discussion

In this article we have shown that intracellular  $\text{Ca}^{2+}$  dynamics, regulated by  $[IP_3]$ , add critical degrees of freedom to a mathematical model of an STG neuron, thereby allowing it to generate irregular bursts that are similar to those observed experimentally. We also analyzed the experimentally observable dynamical variable, namely membrane voltage, using nonlinear tools. Qualitatively and quantitatively, the dynamical characteristics of the model are in close agreement with those observed in earlier experiments.

The model's low-dimensional behavior suggests that we might reduce its 12 dynamical variables to some set of 3 or 4 alone. In fact, our earlier analyses of experimental data led us to use the 3-dimensional model of Hindmarsh and Rose (1984). However, that model lacks clear connections to biological mechanisms and behaves chaotically in only a narrow region of parameter space.

The model presented here suffers from neither drawback. Despite the model's large number of parameters,

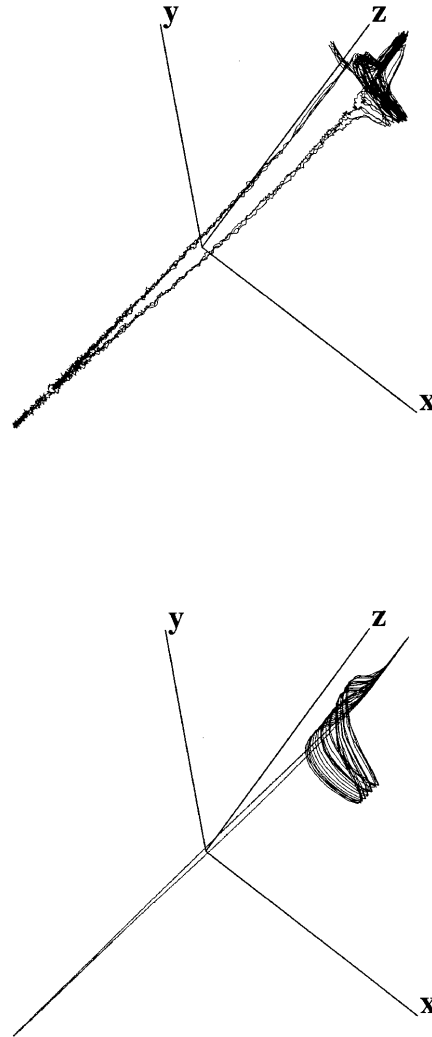


**Fig. 11.** The attractor displayed in three dimensions using reconstructed state space  $\mathbf{y}(n) = [V(t), V(t - T), V(t - 2T)]$  with  $V(t)$  the LP membrane voltage and  $T$  determined from average mutual information. *Top* Evaluated from experimental data. *Bottom* Evaluated from the model with  $IP_3 = 0.354 \mu\text{M}$

its dynamical behavior and its similarities to experimental data suggest the importance of its main feature – namely, a feedback interaction between relatively fast membrane voltage dynamics and a slower intracellular process.

Our work builds on the conductance-based models of STG neurons presented by Buchholtz et al. (1992) and Turrigiano et al. (1995). These models incorporated simple  $\text{Ca}^{2+}$  dynamics consisting of influx via ionic currents and a removal process proportional to the intracellular  $\text{Ca}^{2+}$  concentration. Chaotic bursting-spiking oscillations were reported in neither case. Chay (1996) argued that the  $\text{Ca}^{2+}$  store of the endoplasmic reticulum could be important in regulating bursting behavior, showing that such dynamics allowed chaotic bursting to occur in models of pancreatic  $\beta$ -cells. We have applied this idea to simulations of STG neurons.

In the model described here, membrane  $\text{Ca}^{2+}$  and  $\text{Ca}^{2+}$ -dependent  $\text{K}^+$  currents directly couple the cyto-



solic  $[Ca^{2+}]$  to the membrane voltage. The phase relation between both variables is always preserved in the sense that cytosolic  $[Ca^{2+}]$  always begins to increase when the membrane voltage jumps to the plateau level and reaches a local maximum at the end of the plateau. A similar phase relation has been measured directly in pyloric neurons of the crab STG (Ross et al. 1989).

There is no direct coupling between luminal  $[Ca^{2+}]$  and membrane voltage. This may be the reason why there is no constant phase relation between these variables in the chaotic regime. The aperiodic modulation of cytosolic  $Ca^{2+}$  dynamics by luminal  $[Ca^{2+}]$  leads to irregular behavior. The loss of phase relationship is probably linked to the small-amplitude character of the  $Ca^{2+}$  oscillations. With large-amplitude (a few hundred nM) oscillations, intracellular  $Ca^{2+}$  moves on its intrinsic attractor with a fixed phase difference between luminal and cytosolic  $[Ca^{2+}]$ , and the burst pattern is regular. We do not know whether large amplitude  $Ca^{2+}$  oscillations can occur in the LP neuron. The amplitude of oscillations is obviously influenced not only by the ER, but also by the  $Ca^{2+}$ -buffering capacity of the cytosol and the sequestration of  $Ca^{2+}$  by mitochondria.

We have not attempted a detailed study of the model's transition from regular to chaotic bursting. The bifurcations appear similar to those proposed by Terman (1992). A homoclinic orbit may be present in the calcium subsystem, but this was not investigated.

Our goal was to identify a plausible source of chaotic dynamics that could be sought by experiment. The model remains speculative to the extent that there are, at present, no data concerning  $IP_3$  receptors in STG neurons. However, Zhang et al. (1995) found that caffeine-releasable, intracellular  $Ca^{2+}$  stores could influence  $Ca^{2+}$ -dependent membrane currents in an STG neuron of the crab. In the model, the dominant nonlinear effect enters via  $Ca^{2+}$ -induced  $Ca^{2+}$  release and could therefore also result from the activity of ryanodine receptors. Empirical support for the mechanisms proposed here must come from measurements of intracellular  $[Ca^{2+}]$  and manipulation of  $Ca^{2+}$  metabolism during chaotic bursting.

*Acknowledgements.* The work of Robert Elson and Allen Selverston is supported by NIH grant NS09322. Partial support came also from NSF grants NCR-9612250 and IBN-96334405. Ramón Huerta and Mikhail Rabinovich acknowledge support from U.S. Department of Energy grant DE-FG03-96ER14592. Henry Abarbanel is supported in part by U.S. Department of Energy grant DE-FG03-90ER14138 and in part by NSF grant NCR-9612250. We thank Pablo Varona and Joaquín J. Torres for fruitful discussions.

## Appendix A: Glossary

ER	endoplasmic reticulum
$IP_3$	inositol 1,4,5-trisphosphate
$IP_3R$	$IP_3$ receptor channel of the ER
$C$	cytosolic $Ca^{2+}$ concentration
$C_{er}$	$Ca^{2+}$ concentration in the ER
$h$	inactivation of the $IP_3R$ by $C$
$h_{\infty}(C)$	equilibrium value of $h$

$a_{\infty}(C)$	activation of the $IP_3R$ by $C$
$b_{\infty}(IP_3)$	activation of the $IP_3R$ by $IP_3$
$d_{\infty}(C_{er})$	inactivation of the $IP_3R$ by $C_{er}$
$j_{fil}$	$Ca^{2+}$ uptake of the ER
$j_{rel}$	$Ca^{2+}$ release of the ER
$j_{out}$	$Ca^{2+}$ flux across the cell membrane
$\theta_a$	threshold of the activation of the $IP_3R$ by $C$
$\theta_b$	threshold of the activation of the $IP_3R$ by $IP_3$
$\theta_d$	threshold of the inactivation of the $IP_3R$ by $C_{er}$
$\theta_h$	threshold of the inactivation of the $IP_3R$ by $C$
$k_a(IP_3, C_{er})$	steepness of the dependence of $a_{\infty}$ on $C$
$k_a$	scale factor for $k_a(IP_3, C_{er})$
$k_h(IP_3, C_{er})$	steepness of the dependence of $h_{\infty}$ on $C$
$k_h$	scale factor for $k_h(IP_3, C_{er})$
$k_b(IP_3, C_{er})$	steepness of the dependence of $b_{\infty}$ on $[IP_3]$
$k_d(IP_3, C_{er})$	steepness of the dependence of $d_{\infty}$ on $C_{er}$
$\tau_h(C)$	time constant of $h$ dynamics
$\tau_h, \theta_t, k_t$	parameters of $\tau_h(C)$
$\sigma$	ratio of the effective volume of the ER to the effective volume of the cell: $\frac{V_{er}f_{cyt}}{V_{cell}f_{er}}$
$V_{cell}$	cell volume
$V_{er}$	volume of the ER
$f_{cyt}$	buffering coefficient of the cytosol
$f_{er}$	buffering coefficient of the ER
$V_{erp}, K_{erp}$	maximal pumping rate and half maximum value of $Ca^{2+}$ ATPases of the ER
$P_{leak}$	leak $Ca^{2+}$ flux out of the ER
$P_{IP_3}$	maximum $Ca^{2+}$ flux out of the ER induced by $IP_3$ and $Ca^{2+}$
$v_{pmp}, K_{pmp}$	maximal pumping rate and half maximum value of $Ca^{2+}$ ATPases in the cell membrane
$v_{pmex}, K_{pmex}$	maximal pumping rate and half maximum value of $Ca^{2+}/Na^+$ exchanger in the cell membrane
$V$	soma membrane voltage
$V_1$	axon membrane voltage
$c_m$	soma membrane capacitance
$c_{m1}$	axon membrane capacitance
$I_{Ca1}$	small maximum conductance $Ca^{2+}$ current
$I_{Ca2}$	large maximum conductance $Ca^{2+}$ current
$I_h$	low threshold current
$I_{K(Ca)}$	$Ca^{2+}$ -dependent $K^+$ current
$I_{Na}$	fast $Na^+$ current
$I_{Kd}$	delayed rectifier $K^+$ current
$I_l$	leak current of the soma
$I_{l1}$	leak current of the axon
$I_{V,V1}$	current of ohmic coupling of $V$ and $V_1$
$r_i$	rectification of $I_i$ ; $i$ is Ca1, Ca2, $h$ , K(Ca), Na, Kd, l, l1 or $V, V1$
$g_i$	maximum conductance of $I_i$ ; $i$ is Ca1, Ca2, $h$ , K(Ca), Na, Kd, l, l1, or $V, V1$
$m_i$	activation variable of $I_i$ ; $i$ is Ca1, Ca2, $h$ , K(Ca), Na, or Kd

$\mathbf{h}_i$	inactivation variable of $I_i$ ; $i$ is Ca1 or Na
$\mathbf{e}_{i,m}$	equilibrium value $m_i$
$\mathbf{e}_{i,h}$	equilibrium value $h_i$
$\tau_{i,m}$	time constant of $m_i$ dynamics
$\tau_{i,h}$	time constant of $h_i$ dynamics
$\mathbf{q}_{i,m}$	exponent of the dependence of $I_i$ on $m_i$
$\mathbf{q}_{i,h}$	exponent of the dependence of $I_i$ on $h_i$
$\mathbf{K}_{K(\text{Ca})}$	half maximum value of the $C$ dependence of $e_{K(\text{Ca}),m}$
$\mathbf{f}$	coefficient for the shift of the threshold of $e_{K(\text{Ca}),m}$ by $C$
$\mathbf{F}$	Faraday's constant

$$\Gamma(x, y, z) = \frac{1}{1 + e^{\frac{xy}{z}}} \quad (\text{A7})$$

$$\mathbf{a}_\infty = \Gamma(\boldsymbol{\theta}_a, C, \mathbf{k}_a) \quad (\text{A8})$$

$$\mathbf{b}_\infty = \Gamma(\boldsymbol{\theta}_b, \mathbf{IP}_3, \mathbf{k}_b) \quad (\text{A9})$$

$$\mathbf{d}_\infty = 0.2(1 + 4\Gamma(C_{\text{er}}, \boldsymbol{\theta}_d, \mathbf{k}_d)) \quad (\text{A10})$$

$$\mathbf{h}_\infty = \Gamma(C, \boldsymbol{\theta}_h, \mathbf{k}_h) \quad (\text{A11})$$

$$\mathbf{k}_a = \bar{\mathbf{k}}_a \left( 0.8 + \frac{\mathbf{IP}_3}{\mathbf{IP}_3 + 0.2} \frac{0.15^2}{0.15^2 + (\mathbf{IP}_3 - 0.4)^2} \right) \frac{60}{60 + C_{\text{er}}} \quad (\text{A12})$$

$$\alpha = \frac{\mathbf{f}_{\text{cyt}}}{2\mathbf{FV}_{\text{cell}}}$$

$$\mathbf{k}_h = \bar{\mathbf{k}}_h \left( 0.05 + \frac{\mathbf{IP}_3^2}{\mathbf{IP}_3^2 + 1 + \frac{180}{C_{\text{er}}}} \right) \quad (\text{A13})$$

## Appendix B: The model

### B.1 $\text{Ca}^{2+}$ dynamics

$$\dot{C} = j_{\text{rel}} - j_{\text{fil}} - j_{\text{out}} \quad (\text{A1})$$

$$\dot{C}_{\text{er}} = -(j_{\text{rel}} - j_{\text{fil}})/\sigma \quad (\text{A2})$$

$$\frac{\dot{h}}{\tau_h} = \mathbf{h}_\infty - h \quad (\text{A3})$$

$$j_{\text{fil}} = \mathbf{V}_{\text{erp}} \frac{C^2}{C^2 + \mathbf{K}_{\text{erp}}^2} \quad (\text{A4})$$

$$j_{\text{rel}} = (\mathbf{P}_{\text{leak}} + \mathbf{P}_{\mathbf{IP}_3} \mathbf{a}_\infty \mathbf{b}_\infty \mathbf{d}_\infty h)(C_{\text{er}} - C) \quad (\text{A5})$$

$$j_{\text{out}} = \mathbf{v}_{\text{pmp}} \frac{C^2}{C^2 + \mathbf{K}_{\text{pmp}}^2} + \mathbf{v}_{\text{pmex}} \frac{C^4}{C^4 + \mathbf{K}_{\text{pmex}}^4} + \alpha(I_{\text{Ca1}} + I_{\text{Ca2}}) \quad (\text{A6})$$

$$\tau_h = \frac{\bar{\tau}_h}{b_\infty d_\infty \cosh \frac{C - \theta_t}{k_t}} \quad (\text{A14})$$

### B.2 Voltage dynamics

$$\dot{V} = (-I_{\text{Ca1}} - I_{\text{Ca2}} - I_l - I_{K(\text{Ca})} - I_h - I_{V,V_1})/\mathbf{c}_m \quad (\text{A15})$$

$$\dot{V}_1 = (-I_{\text{Na}} - I_{l1} - I_{Kd} + I_{V,V_1})/\mathbf{c}_{m1} \quad (\text{A16})$$

$$I_i = \mathbf{g}_i \mathbf{m}_i^{\mathbf{q}_{i,m}} \mathbf{h}_i^{\mathbf{q}_{i,h}} \mathbf{r}_i(V) \quad (\text{A17})$$

$$\dot{n}_i = (\mathbf{e}_{i,n} - n_i)/\tau_{i,n}, \quad (n = m, h) \quad (\text{A18})$$

### B.3 Parameters

The voltage values are in mV, the  $\mathbf{g}_i$  in  $\mu\text{S}$ .  $\Gamma(x, y, z)$  is defined in Equation (A7).

$I_i$	$n$	$e_{i,n}$	$q_{i,n}$	$\tau_{i,n}$	$g_i$	$r_i(V)$
$I_{\text{Ca1}}$	$\mathbf{m}$	$\Gamma(-V, 33.1, 13.18)$	3	$60 - 40\Gamma(-V, 53.1, 20.5)$	0.172	$\frac{-V}{\exp\frac{3V}{RT} - 1.0}$
	$\mathbf{h}$	$\Gamma(V, -23.1, 5.5)$	1	150		$\frac{-V}{\exp\frac{3V}{RT} - 1.0}$
$I_{\text{Ca2}}$	$\mathbf{m}$	$\Gamma(-V, -6.9, 17)$	3	$37.14 - 25.86\Gamma(-V, 10.1, 26.4)$	3.75	$\frac{-V}{\exp\frac{3V}{RT} - 1.0}$
$I_{K(\text{Ca})}$	$\mathbf{m}$	$\Gamma(V, 2.5 - f(C - 0.5), -13)x$	1	5/3	0.06	$(V + 80)x$
		$\Gamma(V, -30.5 - f(C - 0.5), -3.5)$				$\frac{C^4}{C^4 + \mathbf{K}_{K(\text{Ca})}^4}$
$I_h$	$\mathbf{m}$	$\Gamma(-V, -43.3, 6.5)$	1	$272 + 1499\Gamma(-V, 27.2, 8.73)$	0.024	$V + 20$
$I_l$					0.0024	$V + 65$
$I_{V,V_1}$					0.072	$V - V_1$
$I_{l1}$					0.024	$V_1 + 65$
	$\mathbf{m}$	$\Gamma(-V_1, 4.5, 5.29)$	3	constant: $m_{\text{Na}} = m_{\text{Naoc}}$	80	$V_1 - 50$
$\mathbf{h}$	$\Gamma(V_1, -28.9, 5.18)$	1	$0.67(1.5 + \Gamma(V_1, -14.9, 3.6))x$			
$I_{Kd}$	$\mathbf{m}$	$\Gamma(-V_1, -7.7, 11.8)$	4	$7.2 - 6.4\Gamma(-V_1, 8.3, 19.2)$	13	$V_1 + 80$

$\sigma = 0.6$ ,  $V_{\text{cell}} = 2.671 \text{ nV}$ ,  $f_{\text{cyt}} = 0.01$ ,  $\theta_a = 0.4 \mu\text{M}$ ,  $\theta_b = 0.6 \mu\text{M}$ ,  $\theta_d = 20 \mu\text{M}$ ,  $\theta_h = 0.36 \mu\text{M}$ ,  $\theta_t = 0.35 \mu\text{M}$ ,  $k_b = 0.2 \mu\text{M}$ ,  $k_d = 10 \mu\text{M}$ ,  $k_t = 0.18 \mu\text{M}$ ,  $\bar{k}_a = 0.14 \mu\text{M}$ ,  $\bar{k}_h = 0.46 \mu\text{M}$ ,  $K_{\text{K}(\text{Ca})} = 0.5 \mu\text{M}$ ,  $K_{\text{erp}} = 0.2 \mu\text{M}$ ,  $K_{\text{pmp}} = 0.1 \mu\text{M}$ ,  $K_{\text{pmex}} = 0.9 \mu\text{M}$ ,  $v_{\text{pmp}} = 0.0145 \mu\text{Ms}^{-1}$ ,  $v_{\text{pmex}} = 0.145 \mu\text{Ms}^{-1}$ ,  $P_{\text{leak}} = 0.0286 \text{ s}^{-1}$ ,  $P_{\text{IP}_3} = 3.571 \text{ s}^{-1}$ ,  $V_{\text{erp}} = 3.762 \mu\text{Ms}^{-1}$ ,  $\bar{\tau}_h = 1.25 \text{ s}$ ,  $\alpha = 0.0194 \mu\text{M} \text{ (nAs)}^{-1}$ ,  $c_m = 0.5 \text{ nF}$ ,  $c_{m1} = 0.33 \text{ nF}$ ,  $f = 2 \text{ V} \mu\text{M}^{-1}$ ,  $F/RT = 0.04095 \text{ mV}^{-1}$ ,  $T = 283 \text{ K}$ .

We have adopted the basic structure of  $I_{\text{K}(\text{Ca})}$  from Buchholtz et al. (1992). We dropped the inhibition of  $I_{\text{K}(\text{Ca})}$  by high  $[\text{Ca}^{2+}]$ , because  $[\text{Ca}^{2+}]$  remains small ( $\approx 0.5 \mu\text{M}$ ) in our simulations. The Hill coefficient for the  $\text{Ca}^{2+}$  dependence was set to 4 in order to make  $I_{\text{K}(\text{Ca})}$  sensitive to smaller amplitudes of  $\text{Ca}^{2+}$ . The parameters of the voltage dependence were fit in order to balance  $I_{\text{Ca}2}$  at the plateau level, to avoid an overshooting of the voltage when  $I_{\text{Ca}1}$  is activated, and to assure a decrease of  $I_{\text{K}(\text{Ca})}$  with decreasing voltage low enough to allow  $I_{\text{Ca}1}$  to activate at trough voltage levels.

We have chosen a rectification according to the Goldman-Hodgkin-Katz theory for the  $\text{Ca}^{2+}$  currents, as recommended by Hille (1992). As a consequence, we adapted the voltage parameters of the steady state values of the activation and inactivation variables of  $I_{\text{Ca}1}$  and  $I_{\text{Ca}2}$  to reach steady state  $I$ - $V$  dependencies typical for low voltage activated (LVA) and high voltage activated (HVA)  $\text{Ca}^{2+}$  currents (see Hille 1992, Chap. 4; Turrigiano et al. 1995).

Parameters such as cell volume and temperature were adapted from published values. The  $\text{Ca}^{2+}$  concentration in the somatic compartment is assumed to be spatially homogeneous.

## References

- Abarbanel HDI (1996) Analysis of observed chaotic data. Springer, Berlin Heidelberg New York
- Abarbanel HDI, Huerta R, Rabinovich MI, Rulkov NF, Rowat P, Selverston AI (1996) Synchronized action of synaptically coupled chaotic model neurons. *Neural Comput* 8: 1567–1602
- Arnold V (1993) Dynamical systems. Springer, Berlin Heidelberg New York
- Bal T, Nagy F, Moulins M (1988) The pyloric central pattern generator in crustacea: a set of conditional neural oscillators. *J Comp Physiol A* 163: 715–727
- Berridge MJ (1987) Inositol trisphosphate and diacylglycerol: two interacting second messengers. *Annu Rev Biochem* 56: 159–193
- Berridge MJ (1993a) Inositol trisphosphate and calcium signaling. *Nature* 361(6410): 315–325
- Berridge MJ (1993b) Elementary and global aspects of calcium signaling. *J Physiol* 499(Pt 2): 290–306
- Bootman MD, Berridge MJ (1995) The elemental principles of calcium signaling. *Cell* 83(5): 675–678
- Buchholtz F, Golowasch J, Epstein R, Marder E (1992) Mathematical model of an identified stomatogastric ganglion neuron. *J Neurophysiol* 67: 332–340
- Chay TR (1996) Electrical bursting and luminal calcium oscillation in excitable cell models. *Biol Cybern* 75: 419–431
- Elson R, Selverston AI, Huerta R, Rulkov NF, Rabinovich MI, Abarbanel HDI (1998) Synchronous behavior of two coupled biological neurons. *Phys Rev Lett* 81: 5691–5695
- Gaponov-Grekhov AV, Rabinovich MI (1992) Nonlinearities in action. Springer, Berlin Heidelberg New York
- Hartline DK, Graubard K (1992) Cellular and synaptic properties in the crustacean stomatogastric nervous system. In: Harris-Warrick RM, Marder E, Selverston AI, Moulins M (eds) *Dynamic biological networks: the stomatogastric nervous system*. MIT Press, Cambridge, Mass., pp 31–85
- Hille B (1992) Ionic channels of excitable membranes, 2nd edn. Sinauer, Sunderland, Mass.
- Hindmarsh JL, Rose RM (1984) A model of neuronal bursting using three coupled first order differential equations. *Proc R Soc Lond B* 221: 87–102
- Keizer J, DeYoung G (1994) Effect of voltage-gated plasma membrane fluxes on  $\text{IP}_3$ -linked  $\text{Ca}^{2+}$  oscillations. *Cell Calcium* 14: 397–410
- Li Y-X, Stojilkovic SS, Keizer J, Rinzel J (1997) Sensing and refilling calcium stores in an excitable cell. *Biophys J* 72: 1080–1091
- Miller JP, Selverston AI (1979) Rapid killing of single neurons by irradiation of intracellularly injected dye. *Science* 206: 702–704
- Mulloney B, Selverston AI (1974) Organization of the stomatogastric ganglion in the spiny lobster. I. Neurons driving the lateral teeth. *J Comp Physiol* 91: 1–32
- Otsu H, Yamamoto A, Maeda N, Mikoshiba K, Tashiro Y (1990) Immunogold localization of inositol 1,4,5-trisphosphate ( $\text{InsP}_3$ ) receptor in mouse cerebellar Purkinje cells using three monoclonal antibodies. *Cell Struct Funct* 15: 163–173
- Pozzan T, Rizzuto R, Volpe P, Meldolesi J (1994) Molecular and cellular physiology of intracellular calcium stores. *Physiol Rev* 74: 595–636
- Ross WN, Graubard K (1989) Spatially and temporally resolved calcium concentration changes in oscillating neurons of crab stomatogastric ganglion. *Proc Natl Acad Sci USA* 86: 1679–1683
- Satoh T, Ross ChA, Villa A, Supattapone S, Pozzan T, Snyder SH, Meldolesi J (1990) The Inositol 1,4,5-trisphosphate receptor in cerebellar Purkinje cells: quantitative immunogold labeling reveals concentration in an ER subcompartment. *J Cell Biol* 111: 615–625
- Takens F (1981) In: Rand D, Young LS (eds) *Dynamical systems and turbulence*. Springer, Berlin Heidelberg New York, pp 366–381
- Terman D (1992) The transition from bursting to continuous spiking in excitable membrane models. *J Nonlinear Sci* 2: 135–182
- Turrigiano G, LeMasson G, Marder E (1995) Selective regulation of current densities underlies spontaneous changes in the activity of cultured neurons. *J Neurosci* 15(5): 3640–3652
- Walton PD, Airey JA, Sutko JL, Beck CF, Mignery GA, Südhof TC, Deerinck TJ, Ellisman MH (1991) Ryanodine and inositol trisphosphate receptors coexist in avian cerebellar Purkinje neurons. *J Cell Biol* 113: 1145–1157
- Zhang B, Wooten JF, Harris-Warwick RM (1995) Calcium-dependent plateau potentials in a crab stomatogastric ganglion motor neuron. II. Calcium-activated slow inward current. *J Neurophysiol* 74: 1938–1946